

# Centrality dependence of elliptic flow and QGP viscosity

A. K. Chaudhuri\*

Variable Energy Cyclotron Centre, 1/AF, Bidhan Nagar, Kolkata 700 064, India

(Dated: February 7, 2020)

Elliptic flow suppression in viscous dynamics is studied in the framework of Israel-Stewart's theory of second order hydrodynamics. Depending on the viscosity to entropy ratio,  $\eta/s=0.08-0.16$ , compared to ideal fluid, in viscous fluid, integrated  $v_2$  is suppressed by  $\sim 5-15\%$ . Comparison with PHOBOS data [1] on integrated  $v_2$  indicate that while central collisions prefer nearly ideal fluid, viscous fluid is demanded in more peripheral collisions. PHENIX data [2] on charged particles elliptic flow also prefer nearly ideal fluid in central collisions and more viscous fluid in peripheral collisions. From a systematic analysis of the PHENIX data, centrality dependence of  $\eta/s$  is obtained. Over a broad range of collision centrality (0-10% - 50-60%),  $\eta/s$  varies between 0-0.17.

PACS numbers: 47.75.+f, 25.75.-q, 25.75.Ld

## I. INTRODUCTION

One of the important results in Au+Au collisions at RHIC is the large elliptic flow in non-central collisions [3, 4, 5, 6]. Large elliptic flows establish that in non-central Au+Au collisions, a collective QCD matter is created. Whether the matter can be characterized as the lattice QCD [7, 8] predicted Quark-Gluon-Plasma (QGP) or not, is still a question of debate. Qualitatively, elliptic flow is naturally explained in a hydrodynamical model, rescattering of secondaries generates pressure and drives the subsequent collective motion. In non-central collisions, the reaction zone is asymmetric (almond shaped), pressure gradient is large in one direction and small in the other. The asymmetric pressure gradient generates the elliptic flow. As the fluid evolves and expands, asymmetry in the reaction zone decreases and a stage arises when the reaction zone becomes symmetric and the system no longer generates elliptic flow. Elliptic flow is an early time phenomenon. It is sensitive to (i) degree of thermalisation, (ii) transport coefficient and (iii) equation of state in the early stage of the fluid [9, 10, 11].

Dissipative effects like viscosity reduce elliptic flow. The conversion of initial spatial anisotropy to momentum anisotropy is hindered in the presence of viscosity and elliptic flow is reduced. QGP viscosity is an important parameter, theoretical estimates of the ratio, (shear) viscosity over the entropy density,  $\eta/s$  cover a wide range, 0.0-1.0. String theory based models (ADS/CFT) give a lower bound on viscosity of any matter  $\eta/s \geq 1/4\pi$  [12]. In perturbative QCD, Arnold et al [13] estimated  $\eta/s \sim 1$ . In a SU(3) gauge theory, Meyer [14] gave the upper bound  $\eta/s < 1.0$ , and his best estimate is  $\eta/s=0.134(33)$  at  $T = 1.165T_c$ . At RHIC region, Nakamura and Sakai [15] estimated the viscosity of a hot gluon gas as  $\eta/s=0.1-0.4$ . Attempts have been made to estimate QGP viscosity directly from experimental data. Gavin and Abdel-Aziz [16] proposed to measure viscosity from transverse mo-

mentum fluctuations. From the existing data on Au+Au collisions, they estimated QGP viscosity as  $\eta/s=0.08-0.30$ . Experimental data on elliptic flow has also been used to estimate QGP viscosity. Elliptic flow scales with eccentricity. Departure from the scaling can be understood as due to off-equilibrium effect and utilized to estimate viscosity [17] as,  $\eta/s=0.11-0.19$ . Experimental observation that elliptic flow scales with transverse kinetic energy is also used to estimate QGP viscosity,  $\eta/s \sim 0.09 \pm 0.015$  [18], a value close to the ADS/CFT bound. From heavy quark energy loss, PHENIX collaboration [19] estimated QGP viscosity  $\eta/s \approx 0.1-0.16$ . Recently, from analysis of RHIC data, in a viscous hydrodynamics, upper bound to viscosity is given  $\eta/s < 0.5$  [20, 21]. In [22], from analysis of  $\phi$  meson multiplicity, mean  $p_T$  and integrated  $v_2$ , QGP viscosity was estimated as  $\eta/s = 0.15 \pm 0.06$ . In a more recent analysis [23], viscosity was estimated as,  $\eta/s = 0.07 \pm 0.03 \pm 0.14$ . In [23], estimate of viscosity was obtained from analyzing STAR data on  $\phi$  mesons multiplicity, mean  $p_T$  and integrated  $v_2$ . In the present paper, we show that centrality dependence of differential elliptic flow requires stronger viscosity in peripheral collisions than in central collisions. PHENIX data [2] on centrality dependence of elliptic flow demand ideal or nearly ideal fluid in central collisions, but in peripheral collisions, more viscous fluid is demanded.

The paper is organized as follows: in section II, we briefly explain the 2nd order Israel-Stewart's theory of dissipative hydrodynamics. Equation of state, initialization of the fluid is described in section III. Results are discussed in section VI. The summary and conclusions are given in section V.

## II. HYDRODYNAMIC MODEL

In the following, we consider a baryon free fluid with only shear viscosity. Bulk viscosity is neglected. In the Israel-Stewart's theory of 2nd order dissipative hydrodynamics, equation of motion of the fluid is obtained by solving,

---

\*E-mail: akc@veccal.ernet.in

$$\partial_\mu T^{\mu\nu} = 0, \quad (1)$$

$$D\pi^{\mu\nu} = -\frac{1}{\tau_\pi}(\pi^{\mu\nu} - 2\eta\nabla^{\langle\mu}u^{\nu\rangle}) - [u^\mu\pi^{\nu\lambda} + u^\nu\pi^{\nu\lambda}]Du_\lambda. \quad (2)$$

Eq.1 is the conservation equation for the energy-momentum tensor,  $T^{\mu\nu} = (\varepsilon + p)u^\mu u^\nu - pg^{\mu\nu} + \pi^{\mu\nu}$ ,  $\varepsilon$ ,  $p$  and  $u$  being the energy density, pressure and fluid velocity respectively.  $\pi^{\mu\nu}$  is the shear stress tensor (we have neglected bulk viscosity and heat conduction). Eq.2 is the relaxation equation for the shear stress tensor  $\pi^{\mu\nu}$ . In Eq.2,  $D = u^\mu\partial_\mu$  is the convective time derivative,  $\nabla^{\langle\mu}u^{\nu\rangle} = \frac{1}{2}(\nabla^\mu u^\nu + \nabla^\nu u^\mu) - \frac{1}{3}(\partial.u)(g^{\mu\nu} - u^\mu u^\nu)$  is a symmetric traceless tensor.  $\eta$  is the shear viscosity and  $\tau_\pi$  is the relaxation time. It may be mentioned that in a conformally symmetric fluid relaxation equation can contain additional terms [24].

Assuming boost-invariance, Eqs.1 and 2 are solved in  $(\tau = \sqrt{t^2 - z^2}, x, y, \eta_s = \frac{1}{2} \ln \frac{t+z}{t-z})$  coordinates, with the code "AZHYDRO-KOLKATA", developed at the Cyclotron Centre, Kolkata. Details of the code can be found in [25]. Within 10% or less, AZHYDRO-KOLKATA simulation reproduces Song and Heinz's [24] result for temporal evolution of momentum anisotropy  $\varepsilon_p$ .

### III. EQUATION OF STATE

Eqs.1,2 are closed with an equation of state (EOS)  $p = p(\varepsilon)$ . Lattice simulations [7, 8] indicate that the confinement-deconfinement transition is a cross over, rather than a 1st or 2nd order phase transition. In Fig.1, a recent lattice simulation [8] for the entropy density is shown. We complement the lattice simulated EOS [8] by a hadronic resonance gas (HRG) EOS comprising all the resonances below mass 2.5 GeV. In Fig.1, the solid line is the entropy density of the "lattice +HRG" EOS. The entropy density is obtained as,

$$s = 0.5[1 - \tanh(x)]s_{HRG} + 0.5[1 + \tanh(x)]s_{lattice} \quad (3)$$

where  $s_{lattice}$  and  $s_{HRG}$  are entropy density from lattice simulations and HRG model,  $x = \frac{T - T_c}{\Delta T}$ . In the present simulation, we have used cross over temperature,  $T_c = 196$  MeV and  $\Delta T = 0.1T_c$ . Compared to lattice simulation, entropy density of HRG drops slowly at low temperature.

### IV. INITIALIZATION OF THE FLUID

Solution of partial differential equations (Eqs.1,2) requires initial conditions, e.g. transverse profile of the energy density ( $\varepsilon(x, y)$ ), fluid velocity ( $v_x(x, y), v_y(x, y)$ ) and shear stress tensor ( $\pi^{\mu\nu}(x, y)$ ) at the initial time  $\tau_i$ . One also need to specify the viscosity ( $\eta$ ) and the relaxation time ( $\tau_\pi$ ). A freeze-out prescription is also needed

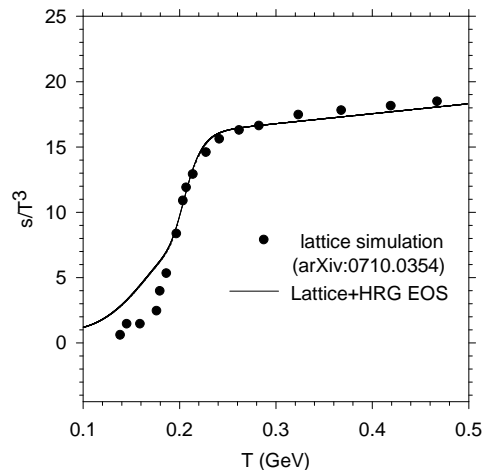


FIG. 1: Lattice simulation for entropy density is compared with the same in the model EOS, lattice+HRG. The filled circles are lattice simulation [8] for  $s/T^3$ . The solid line is the same in the lattice+HRG EOS (see text).

to convert the information about fluid energy density and velocity to particle spectra and compare with experiment.

We assumed that the fluid is thermalised at  $\tau_i = 0.6$  fm [26] and the initial fluid velocity is zero,  $v_x(x, y) = v_y(x, y) = 0$ . Initial energy density is assumed to be distributed as [26]

$$\varepsilon(\mathbf{b}, x, y) = \varepsilon_i [0.75N_{part}(\mathbf{b}, x, y) + 0.25N_{coll}(\mathbf{b}, x, y)], \quad (4)$$

where  $\mathbf{b}$  is the impact parameter of the collision.  $N_{part}$  and  $N_{coll}$  are the transverse profile of the average number of participants and average number collisions respectively, calculated in a Glauber model. Central energy density,  $\varepsilon_i$  is a parameter and does not depend on the impact parameter of the collision. The shear stress tensor was initialized with boost-invariant value,  $\pi^{xx} = \pi^{yy} = 2\eta/3\tau_i$ ,  $\pi^{xy} = 0$ . For the relaxation time, we used the Boltzmann estimate  $\tau_\pi = 3\eta/2p$ . Finally, the freeze-out was fixed at  $T_F = 150$  MeV [27].

TABLE I: Initial central energy density ( $\varepsilon_i$ ) and temperature ( $T_i$ ) of the fluid in  $b=0$  Au+Au collisions, for different values of viscosity to entropy ratio ( $\eta/s$ ). The predicted  $\phi$  meson multiplicity and mean  $p_T$  in 0-5% Au+Au collisions are also noted.

$\eta/s$	$\varepsilon_i$ (GeV/fm <sup>3</sup> )	$T_i$ (MeV)	$\frac{dN^\phi}{dy}$	$\langle p_T \rangle$ (GeV)
0	$35.5 \pm 5.0$	$377.0 \pm 13.7$	7.96	1.02
0.08	$29.1 \pm 3.6$	$359.1 \pm 11.5$	8.01	1.06
0.12	$25.6 \pm 4.0$	$348.0 \pm 14.3$	8.22	1.11
0.16	$20.8 \pm 2.7$	$330.5 \pm 11.3$	8.13	1.17

Assuming that throughout the evolution, viscosity to

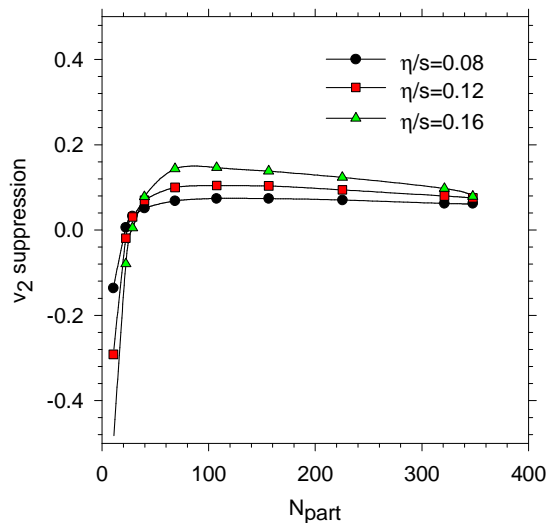


FIG. 2: (color online) Viscous suppression of elliptic flow in Au+Au collisions. The solid, dashed and mid-dashed lines are fractional suppression of elliptic flow in viscous fluid evolution with  $\eta/s=0.08$ ,  $0.12$  and  $0.16$  respectively.

entropy ratio ( $\eta/s$ ) remains a constant, we have simulated Au+Au collisions for four values of  $\eta/s$ , (i)  $\eta/s=0$  (ideal fluid), (ii)  $\eta/s = 1/4\pi \approx 0.08$  (ADS/CFT lower limit of viscosity), (iii)  $\eta/s=0.12$  and (iv)  $\eta/s=0.16$ . Note that during the evolution, the fluid cross over from QGP phase to hadronic phase. Constant  $\eta/s$  can be thought over as a space-time averaged  $\eta/s$ . As the entropy density of the QGP phase is more than that of a HRG (see Fig.1), constancy of  $\eta/s$  during the evolution implicitly assume  $\eta_{QGP} > \eta_{HRG}$ . It also fixes the temperature dependence of  $\eta$ . Variation of  $\eta$  with temperature is the same as that of the entropy density.

Only parameter left to be initialized is the central energy density  $\varepsilon_i$ . We fix  $\varepsilon_i$  such that entropy at the freeze-out is the same either in ideal or in viscous evolution. This is done by reproducing the STAR data [28] on  $\phi$  meson multiplicity in 0-5% Au+Au collisions. In the present work, we have neglected resonance contribution. We choose  $\phi$  meson multiplicity as they are not affected by resonance decays. In table.I, initial central energy density ( $\varepsilon_i$ ) and temperature ( $T_i$ ) required to fit STAR data on  $\phi$  meson multiplicity in 0-5% Au+Au collisions are noted. The error in  $\varepsilon_i$  or in  $T_i$  corresponds to statistical and systematic uncertainty in STAR measurements [28]. In viscous fluid evolution, entropy is generated. More viscous is the fluid, more is the entropy generation. As a consequence, viscous fluid requires less initial energy density (or temperature) than an ideal fluid. For example, compared to ideal fluid, in minimally viscous ( $\eta/s=0.08$ ) fluid, initial energy density is reduced by  $\sim 18\%$ . In fluid with viscosity  $\eta/s=0.16$ , reduction is even more,  $\sim 40\%$ . The predicted central values of  $\phi$  meson multiplicities and mean  $p_T$  are also shown in table.I. They should be compared with STAR measurements [28],

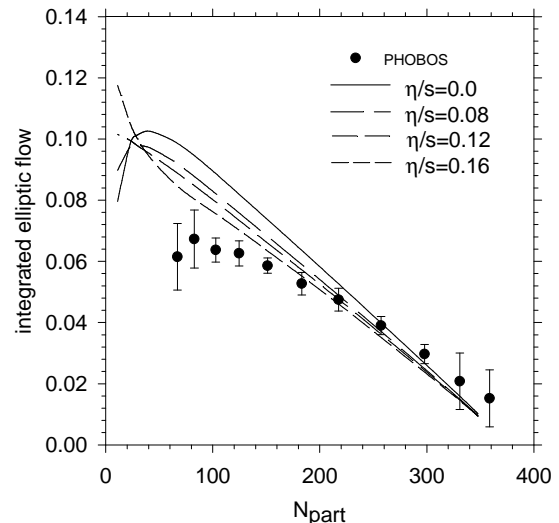


FIG. 3: The filled circles are PHOBOS data [1] on the centrality dependence of charged particles integrated  $v_2$ . The solid, dashed, medium-dashed and short-dashed lines are simulated flow with  $\eta/s=0$ ,  $0.08$ ,  $0.12$  and  $0.16$  respectively.

$\frac{dN^\phi}{dy} = 7.95 \pm 0.74$ , and  $\langle p_T^\phi \rangle = 0.977 \pm 0.064$  (statistical and systematic error included). Experimental data on  $\phi$  meson multiplicity and mean  $p_T$  in 0-5% centrality Au+Au collisions are simultaneously explained only for  $\eta/s \leq 0.12$ . We have not shown it here, but hydrodynamic evolution of the fluid initialized as stated here, reproduce experimental  $p_T$  spectra of pions and kaons at  $p_T > 1$  GeV ( $p_T < 1$  GeV part of the spectra is under-predicted due to neglect of resonance contributions). It also reproduces the  $p_T$  spectra of  $\phi$  mesons. The proton spectra however is underestimated by a factor of  $\sim 2$ .

## V. ELLIPTIC FLOW IN IDEAL AND VISCOUS HYDRODYNAMICS

### A. Centrality dependence of integrated $v_2$

Let us first study the effect of viscosity on  $p_T$  integrated elliptic flow. In Fig.2, fractional decrease in charged particles (pions, kaons and protons) elliptic flow,  $(1 - v_2^{vis}/v_2^{id})$ , as a function of collision centrality is studied. As mentioned earlier, we have neglected resonance decays. Resonance contribution reduces elliptic flow, mostly at low  $p_T$  [29]. Pions are most affected by resonance decays. In the low  $p_T$  range,  $0 \leq p_T \leq 1$  GeV,  $v_2$  is reduced by  $\sim 0$ -30%. At  $p_T > 1$  GeV, resonance contribution to  $v_2$  is negligible [29]. Neglect of resonance contribution will increase integrated  $v_2$ , however, the effect will be minimized in the ratio  $v_2^{vis}/v_2^{id}$ . In collisions with  $N_{part} \geq 100$ , integrated  $v_2$  is suppressed by  $\sim 5\%$ ,  $10\%$  and  $15\%$  for viscosity  $\eta/s=0.08$ ,  $0.12$  and  $0.16$  respectively. There is also an indication that in peripheral collisions,  $v_2$  is more suppressed than in central colli-

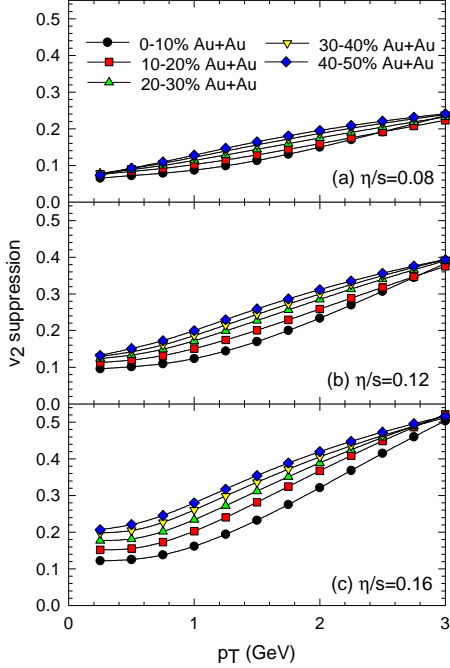


FIG. 4: (color online) Fractional suppression of differential  $v_2$  in Au+Au collisions in the 0-60% centrality ranges of collisions.

sions. In very peripheral collisions,  $N_{part} < 100$ ,  $v_2$  in viscous fluid is more than that in ideal fluid. However, in very peripheral collisions, applicability of hydrodynamics is questionable [26]. We donot think that the present simulations for peripheral collisions are reliable.

In Fig.3, we have compared simulated (integrated) elliptic flow with PHOBOS measurements [1] for charged particles elliptic flow. In Fig.3, the solid, dashed, medium-dashed and short-dashed lines are the charged particles elliptic flow in the present simulation, with  $\eta/s=0, 0.08, 0.12$  and  $0.16$  respectively. Evidently, PHOBOS data on the centrality dependence of  $v_2$  prefer viscous fluid rather than ideal fluid. However, one also note that in central collisions  $N_{part} > 250$ , simulated  $v_2$  in ideal fluid evolution are more close to the experimental data than in viscous evolution. For  $N_{part} > 250$ , data are better explained in ideal dynamics than in viscous dynamics. Data at  $N_{part} < 250$  on the otherhand are better explained in viscous evolution than in ideal evolution.

### B. Centrality dependence of differential $v_2$

Viscous suppression of differential  $v_2$  is studied in Fig.4. In Fig.4, in three panels, for  $\eta/s=0.08, 0.12$  and  $0.16$ , fractional decrease in  $v_2$  in 0-10%, 10-20%, 20-30%,

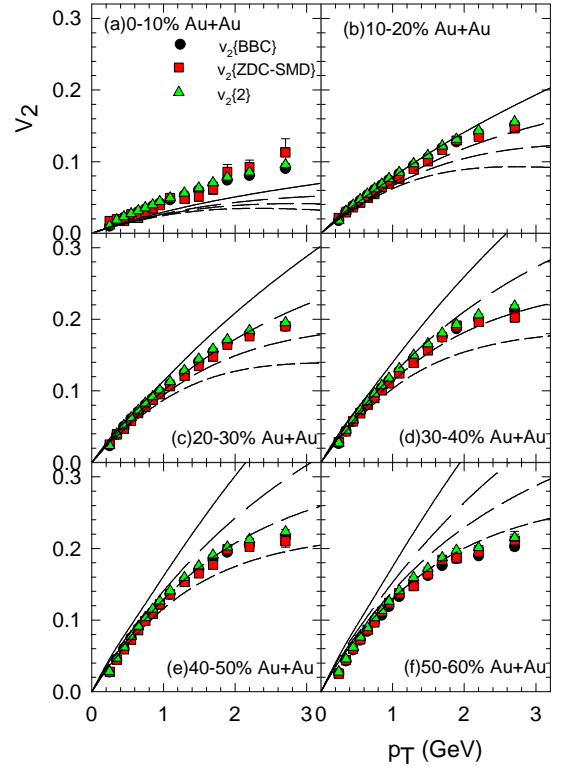


FIG. 5: (color online) In six panels, PHENIX measurements [2] for elliptic flow in 0-10%, 10-20%, 20-30%, 30-40%, 40-50% and 50-60% Au+Au collisions are shown. The solid, dashed, medium dashed and short dashed lines are elliptic flow in hydrodynamic simulations with  $\eta/s=0, 0.08, 0.12$  and  $0.16$  respectively.

30-40% and 40-50% Au+Au collisions are shown. In all the centrality ranges of collisions, viscous suppression is more at high  $p_T$  than at low  $p_T$ . Suppression is also centrality dependent, more in peripheral collisions than in central collisions. For example, for  $\eta/s=0.12$ , at a fixed  $p_T \approx 1$  GeV, compared to a central collisions, in peripheral collisions,  $v_2$  suppression is increased by a factor of  $\sim 2$ . Centrality dependence of viscous suppression is most prominent in the intermediate  $p_T$  range,  $p_T \approx 1-2$  GeV. At large  $p_T$  however, viscous suppression tends to saturate for all collision centrality.

In Fig.5, we have compared the presently simulated  $v_2$  with PHENIX measurements [2]. In Fig.5 colored symbols are PHENIX measurements [2] for charged particles elliptic flow in 0-10%, 10-20%, 20-30%, 30-40%, 40-50% and 50-60% Au+Au collisions. PHENIX collaboration measured charged particles  $v_2$  upto  $p_T \approx 8$  GeV. In Fig.5, measurements upto  $p_T=3$  GeV are shown only. Hydrodynamic models are not well suited for high  $p_T$  particles. In order to study non-flow effects that are not correlated with the reaction plane, as well as fluctuations of  $v_2$ , PHENIX collaboration obtained  $v_2$  from two independent analysis, (i) event plane method from two independent subdetectors,  $v_2\{BBC\}$  and  $v_2\{ZDC-SMC\}$  and (ii) two particle cummulant  $v_2\{2\}$ .  $v_2\{2\}$  from two parti-

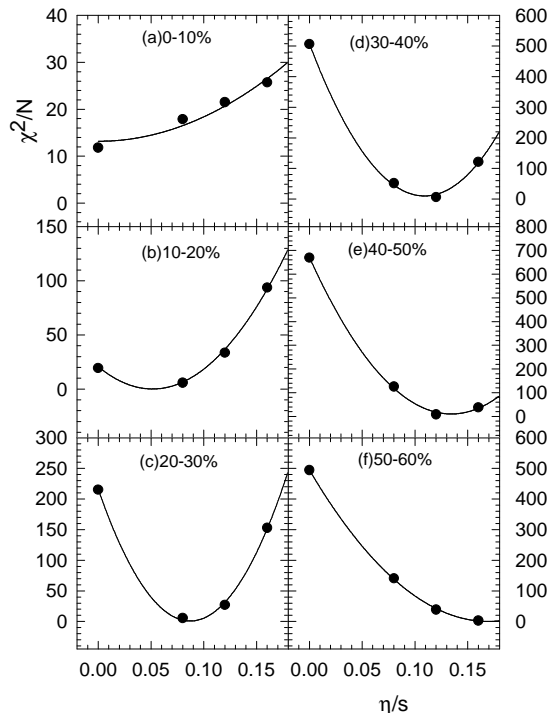


FIG. 6: In six panels,  $\chi^2/N$  for the PHENIX measurements of  $v_2\{2\}$  in 0-10%, 10-20%, 20-30%, 30-40%, 40-50% and 50-60% Au+Au collisions are shown. The solid lines in each panel are fit to the  $\chi^2/N$  values by a parabola.

cle cummulant and  $v_2\{BBC\}$  or  $v_2\{ZDC - BBC\}$  from event plane methods agree within the systematic error. It may also be mentioned here that  $v_2\{2\}$  in PHENIX is lower than that  $v_2\{2\}$  in STAR measurements, but they agree within the systematic error. All the three measurements of  $v_2$  are shown in Fig.5.

In Fig.5, the solid, dashed, medium dashed and short dashed lines are simulated elliptic flow in fluid evolution with (i)  $\eta/s=0$  (ideal fluid), (ii)  $\eta/s=0.08$ , (iii)  $\eta/s=0.12$ , and (iv)  $\eta/s=0.16$ , respectively. Comparison of simulated elliptic flow with PHENIX measurements indicate that in central (0-10%) collisions, hydrodynamic evolution produces less  $v_2$  than in experiment. For example, at  $p_T \approx 1$  GeV, ideal fluid evolution underestimate of PHENIX measurement of  $v_2\{2\}$  by  $\sim 40\%$ . Viscosity reduces  $v_2$  and in viscous evolution  $v_2$  is even more under-predicted. In mid-central or more peripheral collisions, PHENIX data are better explained in viscous fluid evolution than in ideal fluid evolution. To obtain a quantitative idea about the fit obtained to the PHENIX data by the hydrodynamic simulations, we have computed  $\chi^2/N$ ,

$$\chi^2/N = \frac{1}{N} \sum_{i=1}^{i=N} \frac{(EX(i) - TH(i))^2}{ERR(i)^2}. \quad (5)$$

where  $EX(i)$  is the PHENIX measurements for  $v_2\{2\}$  and  $TH(i)$  is the hydrodynamic simulations for  $v_2$ . In

TABLE II: Best fitted  $\eta/s$  as a function of collision centrality. The central temperature ( $T_i$ ) of the fluid are also noted.

coll. centrality	$T_i$ (MeV)	$\eta/s$
0-10%	376.8	$0 \pm 0.03$
10-20%	367.4	$0.051 \pm 0.008$
20-30%	357.9	$0.087 \pm 0.004$
30-40%	350.8	$0.109 \pm 0.003$
40-50%	341.5	$0.134 \pm 0.004$
50-60%	326.7	$0.169 \pm 0.005$

the  $\chi^2/N$  computation, we have included data only the in the  $p_T$  range  $1 \text{ GeV} \leq p_T \leq 3 \text{ GeV}$ . We have neglected resonance production. Resonance contributions lower  $v_2$ , mainly at low  $p_T < 1 \text{ GeV}$  [29]. Present simulations for  $v_2$  below  $p_T < 1 \text{ GeV}$  are not reliable. In Fig.6, in six panels,  $\chi^2/N$  for the six collision centrality studied, are shown as a function of  $\eta/s$ . Except for the very central (0-10%) collision, in all other collision,  $\chi^2/N$  is less in viscous evolution rather than in ideal evolution. In 0-10% centrality collisions, among the four cases studied, minimum  $\chi^2/N$  is obtained in ideal dynamics, even then, the minimum value of  $\chi^2/N$  is 2-5 times higher than that in other collisions. The solid lines in Fig.6 are parabolic fit to  $\chi^2/N$ . We have used CERN MINUIT programme for the fit. From Fig.6, it is evident that the minimum of  $\chi^2$  shifts to higher value of  $\eta/s$  as the collisions become more and more peripheral. From the minimum of the fit, we have extracted the best fitted  $\eta/s$  for each collision centrality. They are noted in table.II.

Best fitted  $\eta/s$  smoothly decreases as the collision become more and more central. While in central collisions, a nearly perfect fluid is produced, more viscous fluid is produced in peripheral collisions. As noted earlier, in a recent work [23], we have estimated QGP viscosity as  $\eta/s = 0.07 \pm 0.03 \pm 0.14$ . The present result that depending on the collision centrality  $\eta/s$  varies between 0-0.17, is consistent with our earlier determination (within the systematic errors).

The empirical finding that the fluid produced in a peripheral Au+Au collision is more viscous than that produced in a central collision, indicates that the ratio,  $\eta/s$  is not a constant as assumed here but depend on the temperature. In table.II, we have noted the initial central temperature of the fluid. In peripheral collisions, the fluid is produced at a lower temperature than in a central collision. Extracted  $\eta/s$  (approximately) linearly decreases with the initial central temperature.

## VI. SUMMARY AND CONCLUSIONS

To summaries, we have studied effect of (shear) viscosity on elliptic flow. To obtain a meaningful comparison between flows in ideal and viscous dynamics, the fluid was initialized to reproduce  $\phi$  meson multiplicity in 0-

5% Au+Au collisions. The initialization ensures that irrespective of fluid viscosity, the final state entropy is the same. Elliptic flow is suppressed in viscous fluid evolution. Depending on viscosity ( $\eta/s=0.08-0.16$ ), in central and mid-central ( $N_{part} \geq 100$ ) collisions, integrated  $v_2$  is suppressed by 5-15% only. PHOBOS data on integrated  $v_2$  also prefer viscous fluid over an ideal fluid. However, it was also indicated that integrated  $v_2$  in more peripheral collisions, demand more viscous fluid than in less peripheral collisions. Elliptic flow in peripheral collisions

demand more viscous fluid is also confirmed from analysis of PHENIX data on charged particles elliptic flow in 0-10%, 10-20%, 20-30%, 30-40% 40-50% and 50-60% centrality collisions. In central collisions (0-20%), PHENIX data are well explained with small viscosity,  $\eta/s \approx 0-0.05$ . In more peripheral collisions, e.g. in 40-60% collisions, data demand more viscous fluid,  $\eta/s \approx 0.13-0.17$ . Centrality dependence of QGP viscosity can be understood if  $\eta/s$  is not a constant but decreases (approximately linearly) with temperature.

- 
- [1] B. B. Back *et al.* [PHOBOS Collaboration], Phys. Rev. C **72**, 051901 (2005)
- [2] S. Afanasiev *et al.* [PHENIX Collaboration], Phys. Rev. C **80**, 024909 (2009) [arXiv:0905.1070 [nucl-ex]].
- [3] BRAHMS Collaboration, I. Arsene *et al.*, Nucl. Phys. A **757**, 1 (2005).
- [4] PHOBOS Collaboration, B. B. Back *et al.*, Nucl. Phys. A **757**, 28 (2005).
- [5] PHENIX Collaboration, K. Adcox *et al.*, Nucl. Phys. A **757** (2005), in press [arXiv:nucl-ex/0410003].
- [6] STAR Collaboration, J. Adams *et al.*, Nucl. Phys. A **757** (2005), in press [arXiv:nucl-ex/0501009].
- [7] Karsch F, Laermann E, Petreczky P, Stickan S and Wetzorke I, 2001 *Proceedings of NIC Symposium* (Ed. H. Rollnik and D. Wolf, John von Neumann Institute for Computing, Jülich, NIC Series, vol.9, ISBN 3-00-009055-X, pp.173-82,2002.)
- [8] M. Cheng *et al.*, Phys. Rev. D **77**, 014511 (2008) [arXiv:0710.0354 [hep-lat]].
- [9] J. Y. Ollitrault, Phys. Rev. D **46**, 229 (1992).
- [10] P. F. Kolb, U. W. Heinz, P. Huovinen, K. J. Eskola and K. Tuominen, Nucl. Phys. A **696**, 197 (2001) [arXiv:hep-ph/0103234].
- [11] T. Hirano and Y. Nara, Nucl. Phys. A **743**, 305 (2004) [arXiv:nucl-th/0404039].
- [12] G. Policastro, D. T. Son and A. O. Starinets, Phys. Rev. Lett. **87**, 081601 (2001).
- [13] P. Arnold, G. D. Moore and L. G. Yaffe, JHEP **0011**, 001 (2000), JHEP **0305**, 051 (2003).
- [14] H. B. Meyer, Phys. Rev. D **76**, 101701 (2007) [arXiv:0704.1801 [hep-lat]].
- [15] A. Nakamura and S. Sakai, Nucl. Phys. A **774**, 775 (2006).
- [16] S. Gavin and M. Abdel-Aziz, Phys. Rev. Lett. **97**, 162302 (2006) [arXiv:nucl-th/0606061].
- [17] H. J. Drescher, A. Dumitru, C. Gombeaud and J. Y. Ollitrault, Phys. Rev. C **76**, 024905 (2007) [arXiv:0704.3553 [nucl-th]].
- [18] R. A. Lacey *et al.*, Phys. Rev. Lett. **98**, 092301 (2007) [arXiv:nucl-ex/0609025].
- [19] A. Adare *et al.* [PHENIX Collaboration], Phys. Rev. Lett. **98**, 172301 (2007) [arXiv:nucl-ex/0611018].
- [20] M. Luzum and P. Romatschke, Phys. Rev. C **78**, 034915 (2008) [arXiv:0804.4015 [nucl-th]].
- [21] H. Song and U. W. Heinz, arXiv:0812.4274 [nucl-th].
- [22] A. K. Chaudhuri, arXiv:0901.0460 [nucl-th].
- [23] A. K. Chaudhuri, arXiv:0909.0391 [nucl-th].
- [24] H. Song and U. W. Heinz, Phys. Rev. C **78**, 024902 (2008) [arXiv:0805.1756 [nucl-th]].
- [25] A. K. Chaudhuri, arXiv:0801.3180 [nucl-th].
- [26] P. F. Kolb and U. Heinz, in *Quark-Gluon Plasma 3*, edited by R. C. Hwa and X.-N. Wang (World Scientific, Singapore, 2004), p. 634.
- [27] We have checked that with the lattice+HRG EOS, in ideal fluid dynamics, STAR measurements of  $\frac{dN^\phi}{dy}$  and  $\langle p_T^\phi \rangle$  in 0-5% Au+Au collisions are best explained with  $T_F=150$  MeV.
- [28] B. I. Abelev *et al.* [STAR Collaboration], Phys. Rev. Lett. **99**, 112301 (2007) [arXiv:nucl-ex/0703033].
- [29] T. Hirano and K. Tsuda, Phys. Rev. C **66**, 054905 (2002) [arXiv:nucl-th/0205043].